Impedance-Based Modelling Method for Length-Scalable Long Transmission Cable for Stability Analysis of Grid-Connected Inverter

Zhou, Weihua; Wang, Yanbo; Chen, Zhe

Published in:
Proceedings of 2018 IEEE 4th Southern Power Electronics Conference (SPEC)

DOI (link to publication from Publisher):
10.1109/SPEC.2018.8635872

Publication date:
2018

Document Version
Accepted author manuscript, peer reviewed version

Impedance-Based Modelling Method for Length-Scalable Long Transmission Cable for Stability Analysis of Grid-Connected Inverter

Weihua Zhou*, Yanbo Wang†, and Zhe Chen‡
Department of Energy Technology
Aalborg University
Aalborg, Denmark
*wez@et.aau.dk, †ywa@et.aau.dk, ‡zch@et.aau.dk

***Abstract*—This paper presents an impedance-based modelling method for length-scalable long transmission cable (LTC), which is able to assess influence of LTC on stability of grid-connected inverter (GCI). Electrical parameters of power cable in per-unit-length (p.u.l.) are first extracted from the measured terminal short-circuited and open-circuited admittances. Then, the terminal admittance of power cable in different length can be derived on the basis of the obtained p.u.l. parameters. Finally, a decoupled two-port circuit model is established for the LTC using the derived terminal admittance. Simulation results are given to validate effectiveness of the proposed impedance-based modelling method for LTC. The proposed impedance-based modelling method is able to avoid repetitive terminal impedance measurement. Also, the proposed model is able to support impedance-based stability criterion for GCI with length-scalable LTC.**

***Index Terms*—Grid-connected inverter, impedance-based stability analysis, long transmission cable, p.u.l. parameters, two-port circuit.**

I. Introduction

The penetration of renewable energy technologies, such as wind and solar power, has been increasing in recent years, due to fossil fuel shortage, climate change and environmental pollution [1], [2]. Because of the abundant wind resources and little visual pollution, large-scale power electronics-dominated offshore wind power plants have been built worldwide, among which grid connected inverter (GCI) and long transmission cable (LTC) are two key components. Distributed parasitic capacitance along the LTC, different from conventional inductive grid, tends to make system oscillate at multiple frequencies, threatening safe and reliable operation [3], [4]. Thus, stability analysis is an important issue in system planning stage.

Impedance-based stability analysis method has been widely proposed to perform stability assessment of power electronics-dominated power plant [5]–[8], where stability is predicted by analyzing whether the ratio of grid impedance and GCI output impedance satisfies the Nyquist stability criterion or not [5]. Existing works have established impedance models of three phase GCIs in dq domain [9], phase domain [10] and sequence domain [11]. Then, Norton equivalent circuit can be established on the basis of derived impedance formula [5]. As for the LTC, most existing works modelled the LTC as cascaded Π circuit instead of modelling it as Norton/ Thevenin equivalent circuit [3], [12], [13]. A decoupled two-port circuit model of LTC is proposed to represent terminal characteristics of power cable, where a voltage controlled voltage source and a current controlled current source are placed at sending end and receiving end, respectively [6]. Compared with conventional circuit model, the decoupled two-port circuit model makes the stability analysis intuitive. However, it is not possible once per-unit-length (p.u.l.) parameters are unknown in advance, since the p.u.l. parameters are required to compute one terminal short-circuited and open-circuited impedance of power cables in different lengths.

Measurement-based p.u.l. parameters estimation methods for LTC have been developed in existing works [14]–[17]. The p.u.l. parameters of multi-conductor cables are extracted from s-parameters which were measured by an advanced vector network analyzer [14]. Though this approach can obtain the p.u.l. parameters, it is mainly used in radio frequency and microwave frequency where signal power and energy considerations are most easily quantified than currents and voltage. It is not suitable for LTC case due to much longer length and much lower resonance frequencies [3]. Phasor measurement unit, supervisory control and data acquisition and wide area measurement system are adopted to measure voltage, current and power at both terminals of transmission lines to identify the p.u.l. parameters [15]–[17]. However, the purpose of the aforementioned p.u.l. parameters estimation methods is state estimation, fault location and accurate relay protection settings, which is not for stability analysis of GCI-LTC system.

This paper proposes a decoupled two-port model for length-scalable cable. First, p.u.l. parameters of a LTC in spe-

This work was supported by the ForskEL and EUDP Project "Voltage Control and Protection for a Grid towards 100% Power Electronics and Cable Network (COPE)" (Project No.: 880063).

978-1-5386-8257-9/18/$31.00 © 2018 European Union

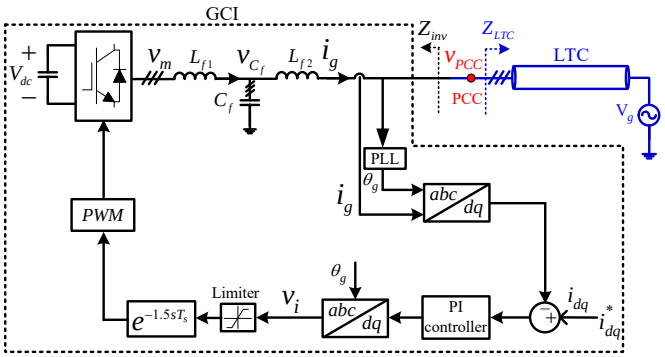

Fig. 1. System diagram of three-phase GCI with LTC.

cific length are extracted from measured one terminal open-circuited and short-circuited admittances. The formulas of one terminal open-circuited and short-circuited impedances of the same kind of LTCs in different lengths are then theoretically calculated based on the derived p.u.l. parameters, and the controlled-source based two-port model is established. Finally, the stability of the original GCI can be assessed by analyzing the stability issue of the equivalent controlled-source-dominated circuit. The main contribution of this paper can be briefly explained as follows. First, the p.u.l. parameters extraction from the measured terminal admittance avoids repetitive terminal impedance measurement of LTCs in different lengths, which is time efficient. Second, the decoupled two-port model of LTC makes the IBSC more convenient and intuitive.

II. System Description and Impedance Model of GCI

Fig. 1 shows a three-phase GCI connected with LTC. Switching harmonic of grid current is eliminated by a LCL filter. In addition, dc-link voltage V_{dc} is considered as constant. The synchronization between grid voltage and inverter output current is realized by a synchronous reference frame phase-locked loop (SRF-PLL). Single grid side current control loop in dq-domain with PI controller is used.

The GCI at the left of PCC can be transferred as Fig. 2(a), where G_{cdq} is the transfer function of PI controller, G_d is digital delay including two components: one sampling period delay T_s for computation, half sampling period delay $0.5T_s$ for PWM modulation, and Y_{LCLl}, Y_{LCLr} are the admittances related to the LCL filter,

$$G_{cdq} = K_p + \frac{K_i}{s} \tag{1}$$

$$G_d = e^{-1.5T_s s} \tag{2}$$

$$Y_{LCLl} = \left.\frac{i_g}{v_m}\right|_{v_{PCC}=0} = \frac{Z_{Cf}}{(Z_{Cf}//sL_{f2} + sL_{f1})(Z_{Cf} + sL_{f2})}$$
$$Y_{LCLr} = \left.\frac{i_g}{v_{PCC}}\right|_{v_m=0} = \frac{1}{(Z_{Cf}//sL_{f1} + sL_{f2})} \tag{3}$$

where $Z_{Cf} = \frac{1}{sC_f}$ is the impedance of capacitance C_f.

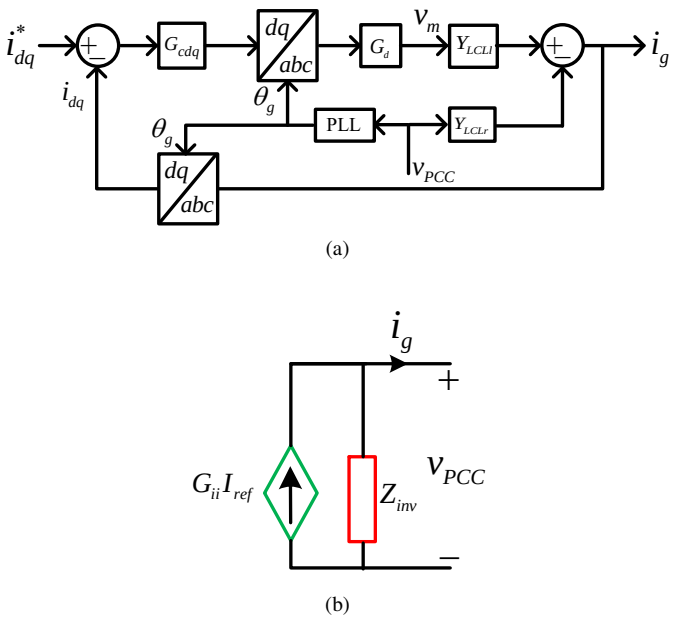

Fig. 2. (a) Block diagram of current control loop in dq domain; (b) Norton equivalent circuit model.

It should be noted that the impact of PLL, dq/abc transformation and abc/dq transformation on output impedance of the GCI can be ignored if PLL bandwidth is small enough [10]. The output impedance equivalent can be derived as,

$$Z_{inv} = -\frac{v_{pcc}}{i_g} = \frac{1 + T_{sys}}{Y_{LCLr}} \tag{4}$$

where $T_{sys} = G_{cdq}G_dY_{LCLl}$ is open-loop gain of the current control loop. The Norton equivalent model can then be obtained, shown as in Fig. 2(b).

III. Proposed Decoupled Two-Port Circuit Modelling Method for Length-Scalable LTC

In this section, basis of LTC is first introduced, and the detailed modelling procedure of proposed decoupled two-port circuit model of LTC is given.

A. Parameters identification of lumped-parameter model of LTC

Voltage and current distribution along uniform LTC/transmission line can be expressed as following classical telegraph equations [18],

$$\partial_x v(x,\omega) = -Z^{'}(\omega) i(x,\omega)$$
$$\partial_x i(x,\omega) = -Y^{'}(\omega) v(x,\omega) \tag{5}$$

where $v(x,\omega)$ and $i(x,\omega)$ are voltage and current at position x of power cable, respectively. $Z^{'}(\omega) = R^{'}(\omega) + j\omega L^{'}(\omega)$ and $Y^{'}(\omega) = G^{'}(\omega) + j\omega C^{'}(\omega)$ are p.u.l. series impedance and shunt admittance of the power cable, respectively. In general, $G^{'}(\omega)$ can be ignored and $C^{'}(\omega)$ can be regarded as constant [18].

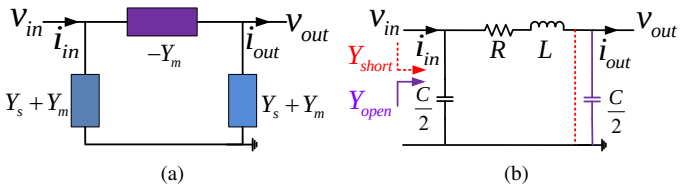

Fig. 3. Single Π model of LTC. (a) Lumped-parameter Π model; (b) Single Π circuit model with RLC components.

To decouple $v(x,\omega)$ and $i(x,\omega)$, (5) is transferred as the following 2-order differential equation,

$$\begin{aligned}\partial_x^2 v(x,\omega) &= Z^{'}(\omega)Y^{'}(\omega)v(x,\omega)) = \gamma(\omega)^2 v(x,\omega)) \\ \partial_x^2 i(x,\omega) &= Z^{'}(\omega)Y^{'}(\omega)i(x,\omega) = \gamma(\omega)^2 i(x,\omega))\end{aligned} \tag{6}$$

where $\gamma(\omega) = \sqrt{(Z^{'}(\omega)Y^{'}(\omega))}$ is the propagation constant which is dependent on p.u.l. parameters of power cable. It means that the same kind of power cables in different lengths have the same value $\gamma(\omega)$. The important characteristics is the basis of the proposed decoupled two-port circuit modelling method for length-scalable LTC, as shown in next section.

As shown in Fig. 3 (a), voltage and current at the receiving end of the LTC $v(out)$, $i(out)$ can be expressed by voltage and current at the sending end of the LTC $v(in)$, $i(in)$ according to the following equation (For simplicity, the symbol ω is omitted in the following analysis),

$$\begin{bmatrix} v_{out} \\ i_{out} \end{bmatrix} = \begin{bmatrix} \Psi_{11} & \Psi_{12} \\ \Psi_{21} & \Psi_{22} \end{bmatrix} \begin{bmatrix} v_{in} \\ i_{in} \end{bmatrix} \tag{7}$$

where $\Psi_{11} = \Psi_{22} = \cosh(\gamma\ell)$, $\Psi_{12} = -Z_c \sinh(\gamma\ell)$ and $\Psi_{21} = -\frac{1}{Z_c}\sinh(\gamma\ell)$. $Z_c = \sqrt{Z^{'}/Y^{'}}$ is the characteristics impedance.

Also, the terminal currents can be expressed by the voltages at both ends, as (8),

$$\begin{bmatrix} i_{in} \\ -i_{out} \end{bmatrix} = \begin{bmatrix} Y_s & Y_m \\ Y_m & Y_s \end{bmatrix} \begin{bmatrix} v_{in} \\ v_{out} \end{bmatrix} \tag{8}$$

where Y_s represents the self-admittance relating the current and voltage at the same end, and Y_m represents the mutual-admittance relating the current and voltage at different ends. They can be expressed as,

$$\begin{aligned} Y_s &= \frac{1}{Z_c \tanh(\gamma\ell)} \\ Y_m &= -\frac{1}{Z_c \sinh(\gamma\ell)} \end{aligned} \tag{9}$$

The formulas of one-end short-circuited admittance Y_{short} and one-end open-circuited admittance Y_{open} can be easily derived from Fig.3 (a), shown as,

$$\begin{aligned} Y_{short} &= Y_s \\ Y_{open} &= (Y_s^2 - Y_m^2)/Y_s \end{aligned} \tag{10}$$

It can be seen from (9) and (10) that Z_c and γ can be extracted if one-end open-circuited admittance Y_{open} and one-end short-circuited admittance Y_{short} of a LTC in specific length are known. The following p.u.l. parameters extraction and decoupled two-port circuit modelling method is based on this.

B. Proposed decoupled two-port circuit modelling method for length-scalable LTC

The proposed decoupled two-port circuit modelling procedure consists of four steps, as shown in Fig. 4. In first step, voltage signal including multiple frequency components is injected into the sending end with receiving end short-circuited. Then, FFT is performed on the corresponding current response at the sending end. The measured admittance values at a set of frequencies $f_i(\mathrm{i} = 1...\mathrm{N})$ can finally be obtained by dividing current responses by injected voltage components. In second step, the one-end open-circuited admittance Y_{open} is obtained in a similar way.

In third step, the p.u.l. resistance $R^{'}$, inductance $L^{'}$ and capacitance $C^{'}$ is extracted from Y_{short} and Y_{open}. By substituting (9) into (10), γ can be calculated as,

$$\gamma = \left(\cosh^{-1}\left(\sqrt{\frac{Y_{short}}{Y_{short}-Y_{open}}}\right) + j2\pi k\right)/\mathrm{d}_0 \quad k \in Z \tag{11}$$

By combining (9) and (10), Z_c can be calculated as,

$$Z_c = \frac{1}{\sqrt{Y_{open}Y_{short}}} \tag{12}$$

Then, p.u.l. series impedance $Z^{'}$ and p.u.l. shunt admittance $Y^{'}$ can be derived as,

$$\begin{aligned} Z^{'} &= R^{'} + j\omega L^{'} = \gamma Z_c = \frac{\gamma}{\sqrt{Y_{open}Y_{short}}} \\ Y^{'} &= j\omega C^{'} = \gamma/Z_c = \gamma\sqrt{Y_{open}Y_{short}} \end{aligned} \tag{13}$$

where $R^{'} = Re(\gamma Z_c)$, $L^{'} = Im(\gamma Z_c)/\omega$ and $C^{'} = Im(\gamma/Z_c)/\omega$.

Step 4 applies the derived γ and Z_c to calculate one-end short-circuited admittance $Y^{'}_{short}$ and one-end open-circuited admittance $Y^{'}_{open}$ of the same type LTC in arbitrary length, and builds its decoupled two-port circuit model. Each terminal of the LTC can be modelled as voltage/current controlled voltage/current source (One terminal has 4 circuit models, and the whole LTC has $4 \times 4 = 16$ circuit models), as shown in Fig. 5 and Fig. 6. Actually, Since the LTC has a strict symmetry characteristics with respect to the plane which is perpendicular to the LTC at middle position [14], the parameters of equivalent circuits of the two ends are the same, which can be seen from Fig. 5 and Fig. 6. The established equivalent circuit model will be used to analyze the stability of GCI-LTC system.

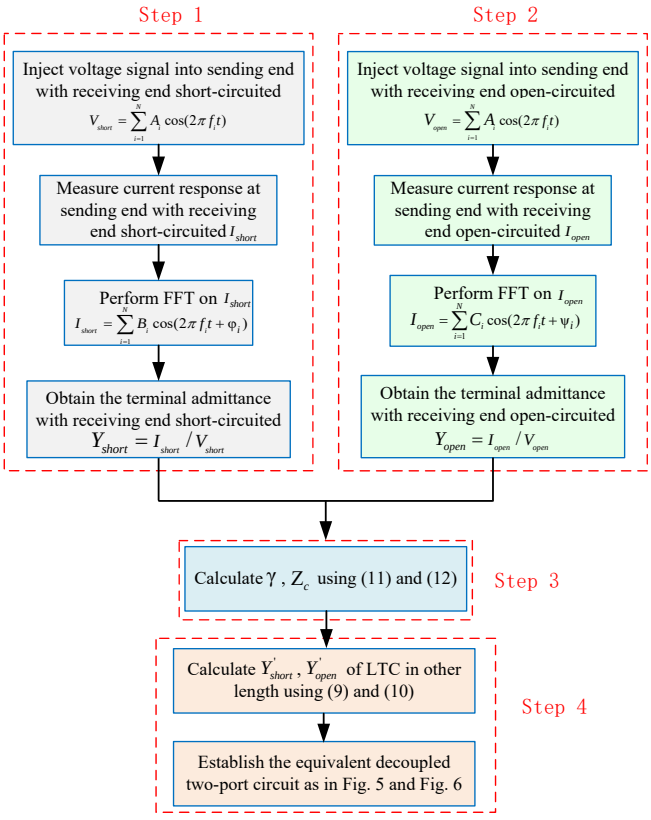

Fig. 4. Flowchart of the proposed decoupled two-port circuit modelling method for length-scalable LTC.

C. Theoretical demonstration of the proposed p.u.l. parameters extraction method

Assuming a LTC with length d_0, p.u.l. resistance R', inductance L' and capacitance C' is studied (The frequency-dependent characteristics of p.u.l. parameters are ignored to simplify the analysis process. However, the conclusion is also applicable when frequency-dependent characteristics is considered, as shown in Section IV). Single Π RLC circuit model can be obtained, shown as in Fig. 3(b). The open-circuited and short-circuited admittances seen from the sending end of the LTC are as,

$$\begin{aligned} Y_{short} &= \frac{1}{sL+R}+\frac{SC}{2} \\ Y_{open} &= \frac{1}{\frac{2}{SC}+sL+R}+\frac{SC}{2} \end{aligned} \tag{14}$$

where $R=R'd_0$, $L=L'd_0$, $C=C'd_0$.

The propagation constant γ_{cal} which is calculated using the proposed method in this paper can be obtained by (11), shown as,

$$\begin{aligned} \gamma_{cal} &= \left(\cosh^{-1}\left(\frac{d_0^2(s^2L'C'+sR'C')}{2}+1\right)+j2\pi k\right)/d_0 \\ &= \left(\cosh^{-1}\left(\frac{d_0^2\gamma_{theo}^2}{2}+1\right)+j2\pi k\right)/d_0 \end{aligned} \tag{15}$$

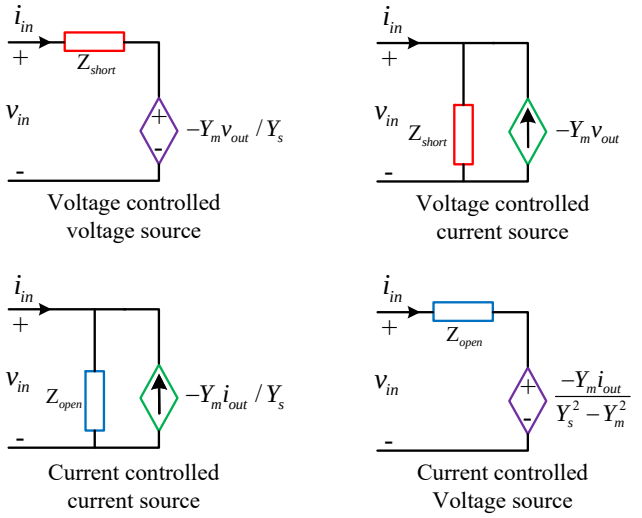

Fig. 5. Four equivalent circuits of sending end of LTC.

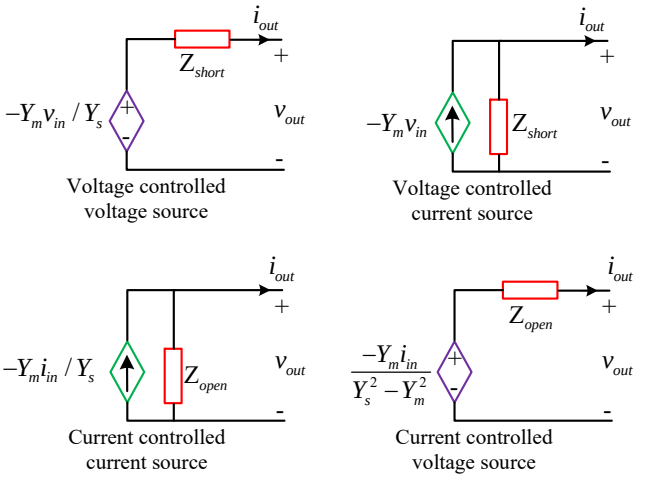

Fig. 6. Four equivalent circuits of receiving end of LTC.

where $\gamma_{theo}=\sqrt{(sL'+R')sC'}$ is the theoretical propagation constant. (15) provides the relationship between the derived propagation constant using terminal admittances and the theoretical propagation constant.

To illustrate the calculation error, the Taylor series expansion of the hyperbolic cosine function $cosh(\gamma_{theo}d_0)$ is shown as,

$$\begin{aligned} \cosh(\gamma_{theo}d_0) &= \frac{e^{\gamma_{theo}d_0}+e^{-\gamma_{theo}d_0}}{2} = 1+\frac{(\gamma_{theo}d_0)^2}{2!} \\ &+\frac{(\gamma_{theo}d_0)^4}{4!}+\frac{(\gamma_{theo}d_0)^6}{6!}\cdots \end{aligned} \tag{16}$$

In principal, infinite cascaded Π sections can reproduce terminal impedance characteristics of the LTC, which means that the LTC length represented by each Π section approximates to 0. Thus, the high-order terms in (16) can be omitted, and

the following equation can be obtained,

$$\gamma_{theo} d_0 \approx \cosh^{-1}(1 + \frac{(\gamma_{theo} d_0)^2}{2!}) + j2\pi k \tag{17}$$

Substituting (17) into (15), it can be found that,

$$\gamma_{cal} \approx \gamma_{theo} = \sqrt{(sL' + R')sC'} \tag{18}$$

It shows that the proposed method can correctly extract the propagation constant γ_{theo} from the measured one-end short-circuited admittance Y_{short} and the measured one-end open-circuited admittance Y_{open}.

IV. Simulation Verification

In this section, simulation verification is performed. Results will be given to show how the p.u.l. parameters of a 100km LTC with consideration of practical frequency-dependent characteristics are extracted, and how the decoupled two-port circuit models of the same kind of LTC in different lengths are established.

The ARTEMIS-SSN library from OPAL-RT provides advanced Modal/Marti and Phase/Wideband frequency dependent line models, which can be easily integrated into Matlab/Simulink model [19]. Therefore, it will be studied in the following p.u.l. parameters extraction and decoupled two-port circuit modelling process.

A. P.u.l. parameters extraction and terminal impedances calculation for length-scalable LTCs

The terminal frequency responses with the other terminal short-circuited and open-circuited Y_{short} and Y_{open} are measured using step 1 and step 2, as shown in Fig. 7.

Then, propagation constant γ can be extracted using (11). It should be noted that the inverse of hyperbolic function in (11) are multi-valued, since any $k \in Z$ satisfies the equation. The derived real part of γ and imaginary part of γ by setting $k = 0$ are shown in Fig. 8(a) and as the blue line in Fig. 8(b), respectively. To recover the actual imaginary part of γ, a pseudo code is shown in Algorithm 1. The recovered imaginary part of γ is shown as the green line in Fig. 8(b).

Algorithm 1: Recover actual imaginary part of γ

```
set f_k as starting point, i = 0 and d_0 as LTC length;
while f_k belongs to the frequency scanning range do
    update γ: imag(γ_knew) = imag(γ_k) + iπ/d_0;
    if the imag(γ_k) equals to π/(2d_0) then
        add 1 to i;
    end
end
```

Finally, p.u.l. parameters $R^{'}$, $L^{'}$, $C^{'}$ can be obtained using (13) with the calculated γ in Fig. 8. The actual and extracted p.u.l. parameters are shown in Fig. 9. It can be seen that they are in good agreement.

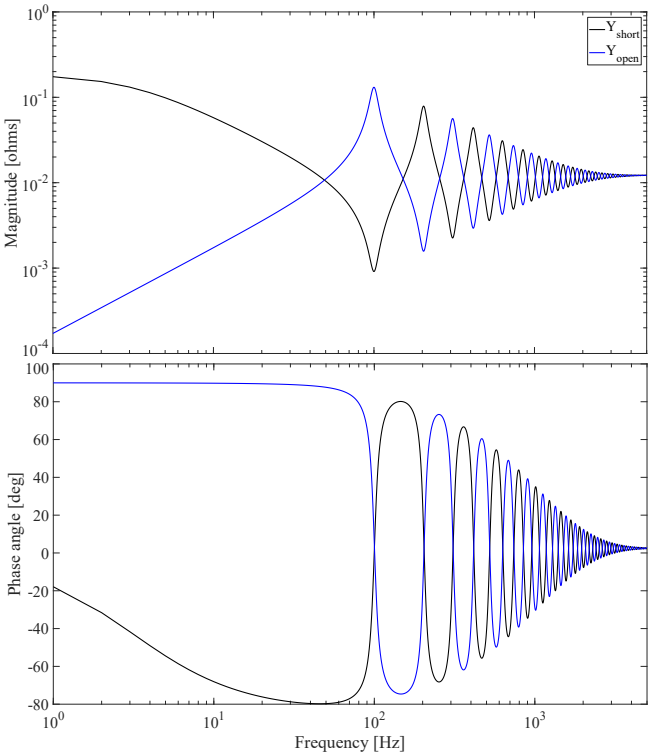

Fig. 7. One-end short-circuited impedance Y_{short} and open-circuited impedance Y_{open} of a 100km LTC.

B. Decoupled two-port circuit models of length-scalable LTCs for stability analysis

Based on the derived p.u.l. parameters, the parameters of equivalent two-port circuits of LTC in arbitrary length in Fig. 5 and Fig. 6 can be calculated using (9) and (10). In principal, the upper two voltage controlled voltage/current sources in Fig. 5 are suitable for modelling the sending end of the LTC, and the lower two current controlled voltage/current sources in Fig. 6 are suitable for modelling the receiving end of the LTC, since GCI output current i_{in} and PCC voltage v_{out} are stable when both the GCI and LTC work in stand alone mode. Therefore, there are four effective impedance models of Fig. 1 for stability analysis, as shown in Fig. 10. It can be seen that the overall system is divided into two parts by using the decoupled impedance model of LTC. The impedance based stability criterion can be performed between the GCI and the sending end of the LTC, and between the receiving end of the LTC and the grid, respectively. In this paper, only stability of the first place should be checked, since the strong grid is assumed. It should be noted that the one terminal short-circuited impedance Z_{short} is calculated by the proposed p.u.l. parameters extraction method instead of repetitive measurement.

The time-domain simulation is performed to verify the effectiveness of the established impedance model of LTC. The electrical parameters of the studied GCI are shown in Table I, and the simulated LTCs have the same p.u.l. electrical parameters as in Fig. 9.

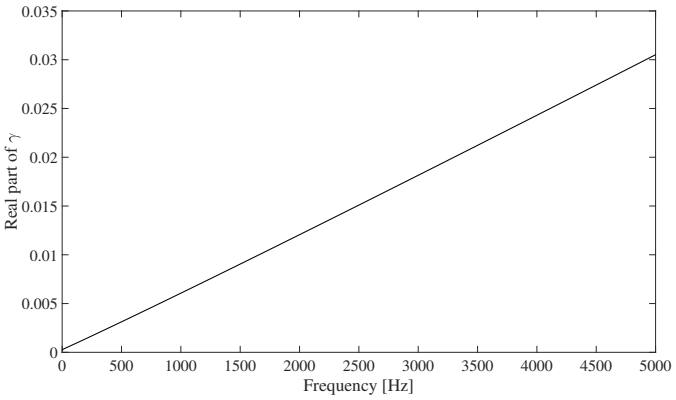

(a)

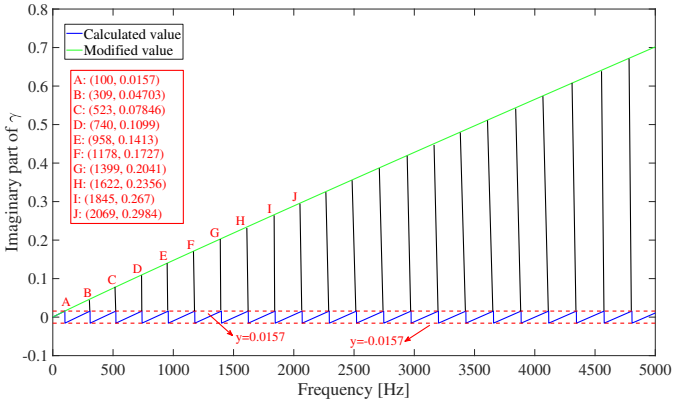

(b)

Fig. 8. Calculated propagation constant γ. (a) Calculated real part of γ; (b) Calculated imaginary part of γ and corresponding recovered values.

TABLE I: System Parameters of the Exemplified Grid-Connected Inverter

Parameter	Value
dc-link voltage V_{dc}	800V
Grid fundamental frequency	50Hz
Filter inductor L_{f1}	$5mH$
Filter inductor L_{f2}	$5mH$
Filter capacitor C_f	$1\mu F$
Switching frquency f_s	10kHz
Sampling frequency f_{samp}	10kHz
Grid voltage (phase-to-phase) V_g	380V
Proportional gain of current controller K_p	40
Integral gain of current controller K_i	2000
Proportional gain of PLL K_p	0.18
Integral gain of PLL K_i	3.2
Magnitude of grid current I_g	30A

The red line in Fig. 11 is the one-end short-circuited impedance of a 10 km LTC, which is derived from the measured terminal admittances of the 100 km LTC, as explained before. Fig. 11 predicts that system is stable, since all the phase differences of the impedance magnitude interactions of GCI and LTC are smaller than 180^o. The time-domain simulation result is shown in Fig. 12. It can be seen from Fig. 11 and Fig. 12 that the derived one-end short-circuited admittance of the 10 km LTC from the calculated p.u.l. parameters can predict

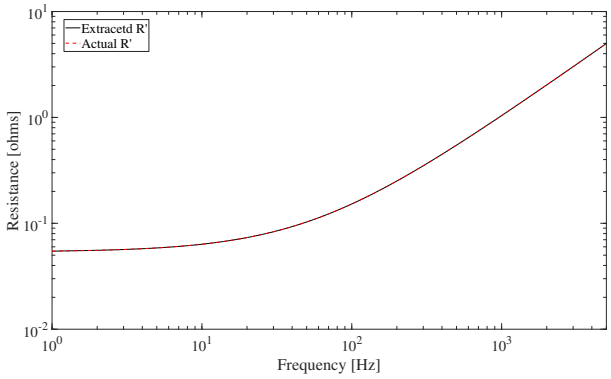

(a)

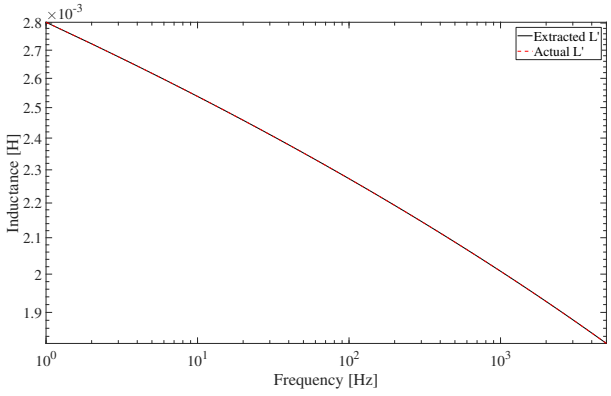

(b)

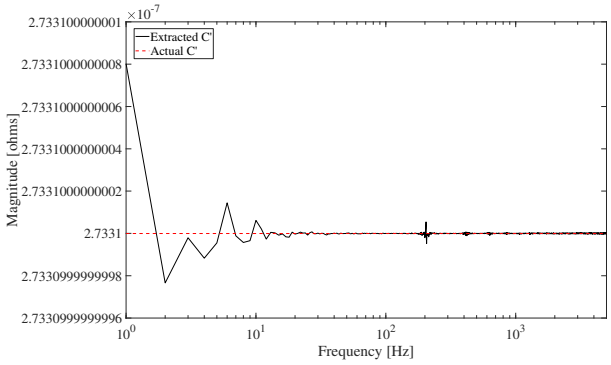

(c)

Fig. 9. Actual and extracted p.u.l. parameters. (a) P.u.l. resistance R'; (b) P.u.l. inductance L'; (c) P.u.l. capacitance C'.

the stability phenomena.

Similarly, the red line in Fig. 13 is the one-end short-circuited impedance of a 6 km LTC, which is derived from the measured terminal admittances of the100 km LTC, as explained before. Fig. 13 predicts that system may be unstable at 2101 Hz, since impedance magnitudes of GCI and LTC are equal, and phase difference is higher than 180^o. The time-domain simulation result and corresponding FFT are shown in Fig. 14. It can be seen from Fig. 13 and Fig. 14 that the derived one-end short-circuited admittance of the 6 km LTC from the calculated p.u.l. parameters can reveal the instability phenomenon.

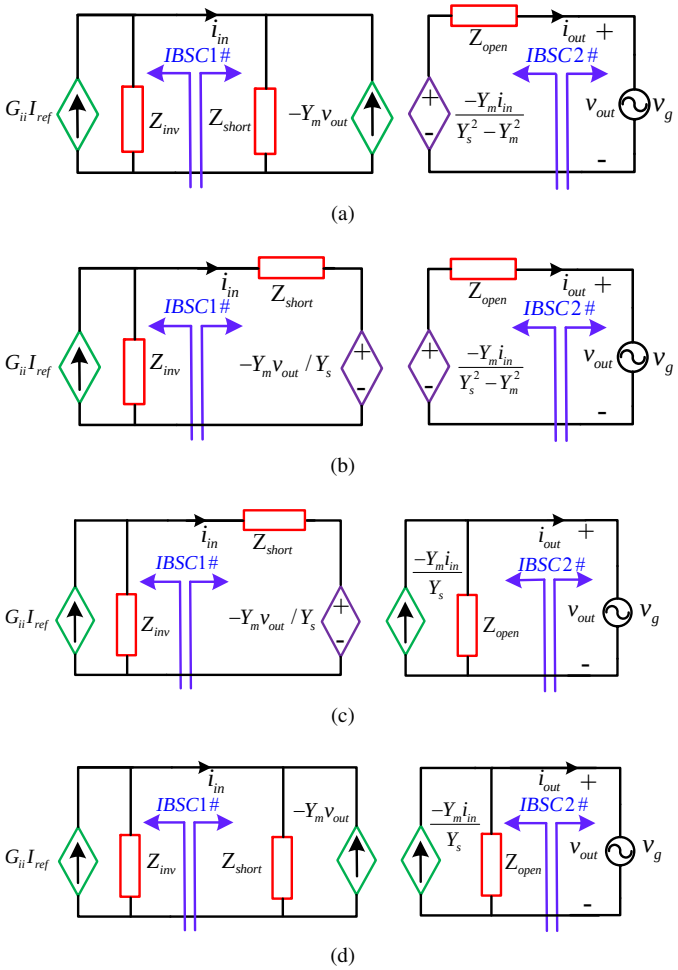

Fig. 10. Impedance models of GCI with LTC. (a) Norton-Norton-Thevenin; (b) Norton-Thevenin-Thevenin; (c) Norton-Thevenin-Norton; (d) Norton-Norton-Norton.

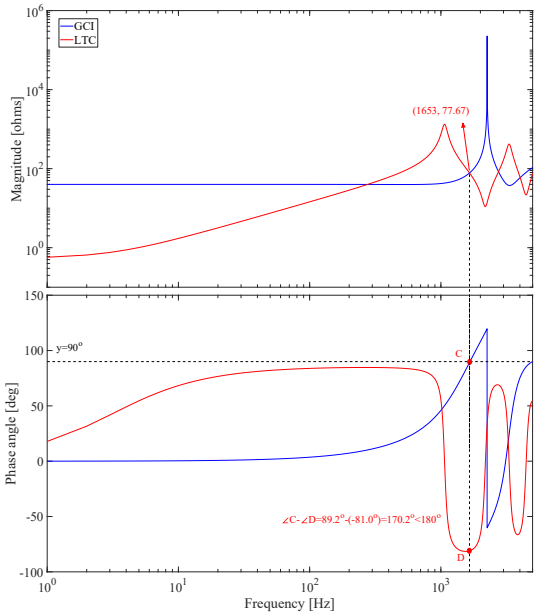

Fig. 11. Bode diagrams of one-end short-circuited impedance of 10 km LTC and GCI output impedance.

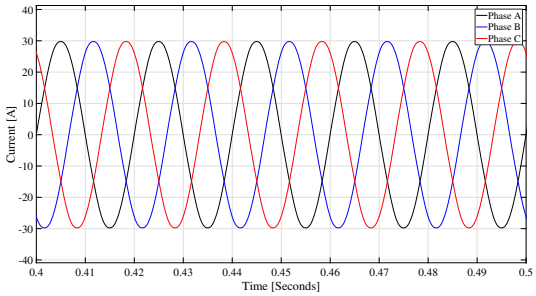

Fig. 12. Time-domain simulation result of grid phase currents when the LTC is 10 km.

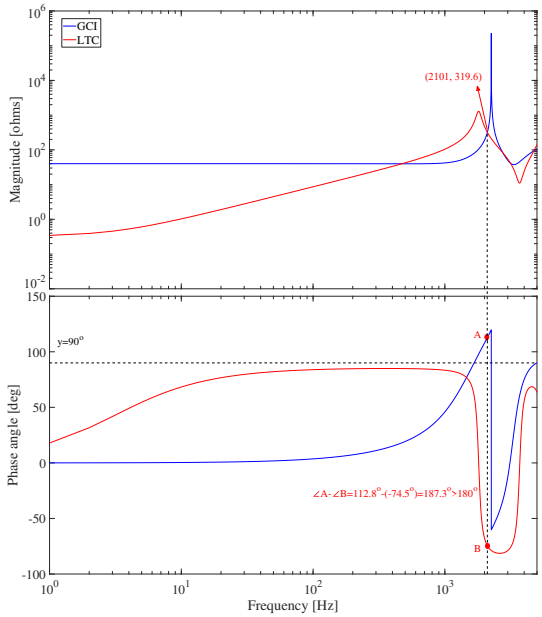

Fig. 13. Bode diagrams of one-end short-circuited impedance of 6 km LTC and GCI output impedance.

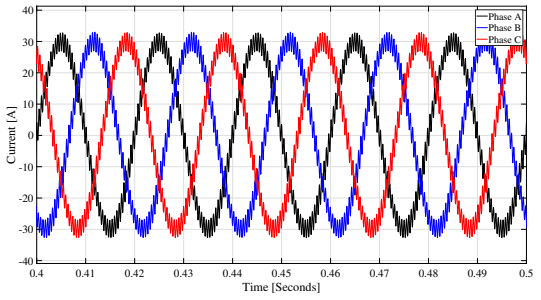

(a)

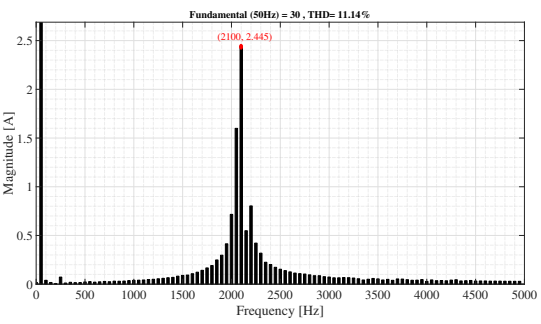

(b)

Fig. 14. Simulation result of grid phase currents when the LTC is 6 km. (a) Time-domain grid phase currents; (b) Frequency spectrum of grid phase currents.

V. Conclusions

The impedance-based modelling method for length-scalable power cable is proposed in this paper. P.u.l. parameters (resistance $R^{'}$, inductance $L^{'}$ and capacitance $C^{'}$) of LTC are first extracted from measured one terminal short-circuit admittance Y_{short} and open-circuit admittance Y_{open}. Then, terminal short-circuited admittance and open-circuited admittance of the same type LTC in different lengths are derived on the basis of the obtained p.u.l. parameters. In addition, the LTC is modelled as a decoupled two-port controlled voltage/current sources. Simulation are performed to verify the effectiveness of the proposed modelling and analysis method. The simulation results show that the p.u.l. parameters can be accurately extracted by the proposed method, and the established decoupled two-port model can predict the system stability.

The proposed p.u.l. parameters extraction and two-port modelling method for LTC have the following two merits. First one is that repetitive measurement of terminal admittances of LTCs in different lengths is avoided. Second one is that the LTC is modelled as controlled voltage/current sources which are similar to the equivalent circuit model of GCI, unifying the representation of system components and facilitating the IBSC.

References

[1] Z. Chen, J. M. Guerrero, and F. Blaabjerg, "A review of the state of the art of power electronics for wind turbines," *IEEE Trans. Power Electron.*, vol. 24, no. 8, pp. 1859–1875, Aug. 2009.

[2] N. Flourentzou, V. G. Agelidis, and G. D. Demetriades, "VSC-based HVDC power transmission systems: An overview," *IEEE Trans. Power Electron.*, vol. 24, no. 3, pp. 592–602, Mar. 2009.

[3] S. Zhang, S. Jiang, X. Lu, B. Ge, and F. Z. Peng, "Resonance issues and damping techniques for grid-connected inverters with long transmission cable," *IEEE Trans. Power Electron.*, vol. 29, no. 1, pp. 110–120, Jan. 2014.

[4] W. Zhou, Y. Wang, and Z. Chen, "Reduced-order modelling method of grid-connected inverter with long transmission cable," in *Proc. 44th IEEE Annual Conference on Industrial Electronics Society*. IEEE, 2018, pp. 1–7.

[5] J. Sun, "Impedance-based stability criterion for grid-connected inverters," *IEEE Trans. Power Electron.*, vol. 26, no. 11, pp. 3075–3078, Nov. 2011.

[6] X. Zhang, H. S.-h. Chung, L. L. Cao, J. P. W. Chow, and W. Wu, "Impedance-based stability criterion for multiple offshore inverters connected in parallel with long cables," in *Proc. Energy Convers. Congr. and Expo.* IEEE, 2017, pp. 3383–3389.

[7] Y. Wang, X. Wang, F. Blaabjerg, and Z. Chen, "Harmonic instability assessment using state-space modeling and participation analysis in inverter-fed power systems," *IEEE Trans. Ind. Electron.*, vol. 64, no. 1, pp. 806–816, Jan. 2017.

[8] W. Zhou, Y. Wang, and Z. Chen, "Decoupled multi-port impedance modelling method of transmission network in inverter-fed power plant," in *Proc. 6th International Conference On Smart Grid*. IEEE, Accepted.

[9] B. Wen, R. Burgos, D. Boroyevich, P. Mattavelli, and Z. Shen, "AC stability analysis and dq frame impedance specifications in power-electronics-based distributed power systems," *IEEE J. Emerg. Sel. Topics Power Electron.*, vol. 5, no. 4, pp. 1455–1465, Dec. 2017.

[10] A. Rygg, M. Molinas, C. Zhang, and X. Cai, "On the equivalence and impact on stability of impedance modeling of power electronic converters in different domains," *IEEE J. Emerg. Sel. Topics Power Electron.*, vol. 5, no. 4, pp. 1444–1454, Dec. 2017.

[11] M. Cespedes and J. Sun, "Impedance modeling and analysis of grid-connected voltage-source converters," *IEEE Trans. Power Electron.*, vol. 29, no. 3, pp. 1254–1261, Mar. 2014.

[12] H. Wang, T. Saha, and R. Zane, "Impedance-based stability analysis and design considerations for DC current distribution with long transmission cable," in *Proc. Control and Modeling for Power Electronics (COMPEL)*. IEEE, 2017, pp. 1–8.

[13] Y. Song, E. Ebrahimzadeh, and F. Blaabjerg, "Analysis of high frequency resonance in DFIG-based offshore wind farm via long transmission cable," *IEEE Trans. Energy Convers.*, 2018, Early Access.

[14] B. Wunsch, I. Stevanović, and S. Skibin, "Length-scalable multiconductor cable modeling for EMI simulations in power electronics," *IEEE Trans. Power Electron.*, vol. 32, no. 3, pp. 1908–1916, Mar. 2017.

[15] C. Li, Y. Zhang, H. Zhang, Q. Wu *et al.*, "Measurement-based transmission line parameter estimation with adaptive data selection scheme," *IEEE Trans. Smart Grid*, Early Access.

[16] P. Ren, H. Lev-Ari, and A. Abur, "Tracking three-phase untransposed transmission line parameters using synchronized measurements," *IEEE Trans. Power Syst.*, vol. 33, no. 4, pp. 4155–4163, Jul. 2018.

[17] V. Milojević, S. Čalija, G. Rietveld, M. V. Ačanski, and D. Colangelo, "Utilization of PMU measurements for three-phase line parameter estimation in power systems," *IEEE Trans. Instrum. Meas.*, no. 99, pp. 1–10, Jun. 2018.

[18] C. R. Paul, *Analysis of multiconductor transmission lines*. John Wiley & Sons, 2008.

[19] ARTEMiS SSN library, https://www.opal-rt.com/solver-artemis-ssn/, accessed: 2018-07-25.